CHINESE OPTICS LETTERS

Vol. 22, No. 5 | May 2024

Multi-focus non-periodic scanning method for femtosecond lasers based on DMD and galvanometer scanners [Invited]

Huaming Li (李华明)[1,2,†], Yu Wang (王 雨)[1,2,†], Qinglei Hu (胡庆磊)[1,2], Zhuoyu Zhang (张卓宇)[1,2], Xiaohua Lü (吕晓华)[1,2], and Shaoqun Zeng (曾绍群)[1,2*]

[1] Britton Chance Center for Biomedical Photonics, Wuhan National Laboratory for Optoelectronics, Huazhong University of Science and Technology, Wuhan 430074, China

[2] MOE Key Laboratory for Biomedical Photonics, Collaborative Innovation Center for Biomedical Engineering, School of Engineering Sciences, Huazhong University of Science and Technology, Wuhan 430074, China

[†]These authors contributed equally to this work.

*Corresponding author: sqzeng@mail.hust.edu.cn

Received October 9, 2023 | Accepted February 5, 2024 | Posted Online May 17, 2024

Multi-focus parallel scanning can effectively increase laser fabrication throughput. However, the conventional approach of using a spatial light modulator (SLM) to generate multi-foci and scan this fixed number of foci with galvanometer scanners can only achieve a periodic scanning trajectory due to the low switching speed of the SLM. Here we demonstrate a multi-focus non-periodic scanning method for femtosecond lasers by using, instead, a fast-switching digital micromirror device (DMD) to generate a dynamic number of foci. The number of effective foci is quickly switched by introducing aberration to the undesired focus. In this way, the intensity allocated to each focus will not be affected by the number of foci, and a uniformity of 98% with different numbers of foci is achieved without adjusting the total laser energy. Finally, we validate the effectiveness of this scanning method by demonstrating corneal flap fabrication of porcine cornea *in vitro*.

Keywords: multi-focus; non-periodic trajectory; digital micromirror device; aberration control; corneal cutting.
DOI: 10.3788/COL202422.051701

1. Introduction

Femtosecond lasers are widely used in microfabrication[1,2], biological imaging[3-7], and optical storage[8,9] due to their nonlinear optical effects. Generally, the femtosecond laser beam is focused to achieve a high peak power density for nonlinear optical effects, which means that it is only suitable for point scanning. However, the low scanning throughput of point scanning limits the application of the femtosecond laser. One of the methods to improve scanning throughput is multi-focus parallel scanning. Conventional optical devices that produce multi-points include the micro lens array (MLA), cascaded beam splitters (CBSs), diffraction optical elements (DOEs), acousto-optic deflectors (AODs), and spatial light modulators (SLMs). The MLA and CBS can simply generate multiple foci[10,11], but the uniformity of the focus intensity is poor. The multi-focus generated by the DOE can possess superior intensity uniformity[12], but because it is a diffractive element, it will have an angular dispersion effect when applied to the femtosecond laser. In addition, the MLA, CBS, and DOE are passive components, and the number and distribution of foci generated by them cannot be changed, so they lack flexibility in application. The AOD can change the number and distribution of foci by adjusting its loaded actuation signal[13,14], which is more flexible than passive components but needs to solve the problems of time and spatial dispersion. At present, a more common method for generating multi-focus is to display a computer-generated hologram (CGH) on SLM[15,16], which has high diffraction efficiency and optical modulation ability. However, due to the refresh rate of SLM being around 100 Hz, it is usually necessary to use it in conjunction with fast scanning components such as a galvanometer scanner, and the scanning trajectory can only be of a periodic structure, resulting in a loss of flexibility. Recently, research on multi-focus non-periodic scanning for femtosecond lasers has also developed. Geng *et al.* used the digital micromirror device (DMD), which can be seen as a special SLM with a refresh rate of up to 32 kHz, as both a scanner and a multi-focus generator. By switching the holograms displayed on the DMD, multi-focus parallel aperiodic scanning can be achieved[17], but the scanning throughput is lower compared to the method of SLM combined with the galvo scanners. To solve the scanning

flux problem, Jiao *et al.* proposed a method that combines scanning and projection methods, using the AOD as the scanner, the DOE as the multi-focus generator, and the DMD as the digital mask[18]. Yang *et al.* advanced a method of combining the DMD with the MLA, where the DMD acts as a digital mask to change the number and distribution of multiple points generated by the MLA[19].

In this Letter, we propose a new multi-focus non-periodic trajectory scanning method for femtosecond lasers based on DMD and galvo scanners. By loading different binary holograms, the DMD can generate and control one to dozens of foci, simultaneously. During the scanning process of the galvo scanners, the number of foci is constantly changing during the scanning process by rapid switching of the displayed hologram on the DMD, enabling the scanning of complex aperiodic structures. However, the regular method of changing the number of foci based on diffraction results in a change in intensity of focus, which leads to uneven processing quality. Here, we present a method to change the foci number by controlling aberration. It will significantly improve the intensity uniformity of foci arrays with different numbers.

2. Methods and Experimental Results

The principle of multi-focus non-periodic trajectory scanning for femtosecond lasers based on DMD and galvo scanners is shown in Fig. 1. Take scanning a triangle by four foci as an example. First, four foci distributed in a linear array are generated through the DMD, and the galvo scanners cause these foci to be moved parallel in the same direction. Second, when the red focus is scanned outside the triangular area, quickly switch the hologram loaded on the DMD that will change the number of foci to 3 (the red focus is "off"). By analogy, as shown in Fig. 1(a), once the foci are out of the target scanning area, the hologram will be switched to make these foci "off." Similarly, when the foci enter the target scanning area, switch the hologram to make these foci "on," as shown in Fig. 1(b). Finally, the scanning trajectory of the triangle area as shown in Fig. 1(c) is realized.

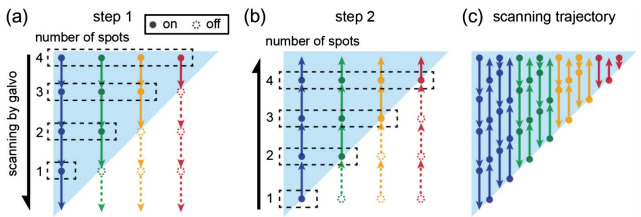

Fig. 1. Schematic for multi-focus non-periodic trajectory scanning for a femtosecond laser based on DMD and galvo scanners. (a) The blue area is the target scanning area. The galvo scanners cause foci to achieve raster scanning, and the DMD controls the "on or off" of each of the four foci by quickly transforming the hologram. (b) Scanning control in the other direction of raster scanning. When foci enter the target area, the foci are turned "on." (c) Final scanning trajectory.

High-intensity uniformity foci array generation is a key issue of the multi-focus scanning system, which determines the quality of high-precision fabrication. Using the same CGH method to generate multiple foci, the total diffraction efficiency is fixed, which means that the change in the foci amount will lead to a change in energy allocated to each focus. For example, each focal energy of two foci generated by the hologram is twice that of four foci. To solve this problem, a common way is to add energy-adjusting devices to the optical system, such as an acoustic-optic modulator (AOM) and electro-optic modulator (EOM), to quickly adjust the energy of the laser beam. However, due to the addition of these devices, the system complexity and system control difficulty increase. In this paper, we propose a method to independently control the "on and off" of each focus through aberration. Aberrations of the foci that need to be "on" are corrected to increase the focus energy density, and aberrations are introduced into the foci that need to be "off" to reduce the focus energy density. Because of the threshold effect and nonlinear effect of the femtosecond laser, the energy density of "off" focus cannot reach the processing threshold energy density, so it has no processing effect. In this method, the number of foci generated by each hologram does not change, so there are unnecessary additional energy modulators for adjusting the diffraction energy of different holograms.

Generally, the holograms that generate different numbers and distributions of focal points can be directly calculated by the weighted Gerchberg–Saxton (GSW) algorithm[20]. As shown in Eq. (1), the phase value corresponding to the jth pixel of the hologram generating K foci after the nth iteration is

$$\varnothing_j^{(n)} = \arg\left\{\sum_{k=1}^{K} w_k^{(n)} e^{i[\varphi_k(x_j,y_j)+\theta_k^{(n)}]}\right\}, \tag{1}$$

where $\varphi_k(x_j, y_j)$ is the phase of the kth focus. The iteration proceeds of weight $w_k^{(n)}$ and phase $\theta_k^{(n)}$ are as follows:

$$w_k^{(n)} = w_k^{(n-1)} \frac{\frac{1}{K}\sum_{k=1}^{K}|E_k^{(n-1)}|}{|E_k^{(n-1)}|}, \tag{2}$$

$$\theta_k^{(n)} = \arg(E_k^{(n-1)}). \tag{3}$$

The initial value of iteration $w_k^{(0)} = 1/K$, and $\theta_k^{(0)}$ is a random phase. $E_k^{(n-1)}$ is the complex amplitude of the kth focus after the $(n-1)$th iteration. In pure phase modulation, the calculation expression for $E_k^{(n)}$ is

$$E_k^{(n)} = \sum_{j=1}^{N} \frac{1}{N} e^{i[\varnothing_j^{(n)} - \varphi_k(x_j,y_j)]}. \tag{4}$$

The DMD is a binary amplitude modulator; thus, the phase modulation $\varnothing_j$ needs to be transformed into amplitude modulation via Lee holography[21]. The DMD-generated amplitude modulation $H_j(x_j, y_j)$ is expressed as

$$H_j(x_j, y_j) = \begin{cases} 1, & \left|\frac{\varnothing_j(x_j, y_j)}{2\pi} + b\right| < \frac{1}{4}, \\ 0, & \text{otherwise} \end{cases} \tag{5}$$

where b is an integer. Therefore, the calculation expression for $E_k^{(n)}$ is modified to

$$E_k^{(n)} = \sum_{j=1}^{N} \frac{1}{N} H_j(x_j, y_j) e^{i[-\varphi_k(x_j, y_j)]}. \tag{6}$$

In this paper, in order to achieve focus "on or off" through aberration control, the focus phase is the sum of the scanning phase and the aberration correction phase, namely,

$$\varphi_k(x_j, y_j) = \varphi_{\text{scan},k}(x_j, y_j) + \varphi_{\text{AO},k}(x_j, y_j), \tag{7}$$

where

$$\varphi_{\text{scan},k}(x_j, y_j) = \frac{2\pi(x_j x_k + y_j y_k)}{\lambda f} + \frac{z_k \pi(x_j^2 + y_j^2)}{\lambda f^2} \tag{8}$$

is the scanning phase of the kth focus, and

$$\varphi_{\text{AO},k}(x_j, y_j) = \sum_{a=4}^{15} c_a Z_a\left(\frac{\rho}{\rho_0}, \theta\right) \tag{9}$$

is the aberration correction phase of the corresponding focus, where

$$\begin{cases} \rho = \sqrt{x_j^2 + y_j^2}, \\ \theta = \arctan(y_j / x_j), & x_j \geq 0 \cdot \\ \theta = \arctan(y_j / x_j) + \pi, & x_j < 0 \end{cases} \tag{10}$$

(x_k, y_k, z_k) represents the kth focus coordinates. c_a is the Zernike coefficient of the ath Zernike mode, and ρ_0 is the radius of the objective lens pupil. Previously, we have demonstrated the obtained Zernike coefficient $c_{a,\text{best}}$ for aberration correction through iterative algorithms[22]. In this way, when we make $c_a = -c_{a,\text{best}}$ in Eq. (9), the focus will introduce a huge aberration, achieving focus "off."

The GSW algorithm, which is improved and applied to generate binary holograms in this article, is called the GSW for binary (GSW-B) algorithm. The intensity uniformity of multi-focus generated by binary holograms that are directly calculated using the GSW-B is low. To improve the uniformity of intensity, the hologram is adjusted through true focal intensity captured by the camera. As shown in Fig. 2, the actual light intensity is fed back to calculate the weight scaling factor $g_k^{(m)}$. The expression for calculating the phase of a hologram is

$$\varnothing_j^{(n)} = \arg\left\{\sum_{k=1}^{K} g_k^{(m)} w_k^{(n)} e^{i[\varphi_k(x_j, y_j) + \theta_k^{(n)}]}\right\}, \tag{11}$$

where m is the number of times that the camera has feedback, and the initial value $g_k^{(0)}$ of $g_k^{(m)}$ is 1. During the iteration process,

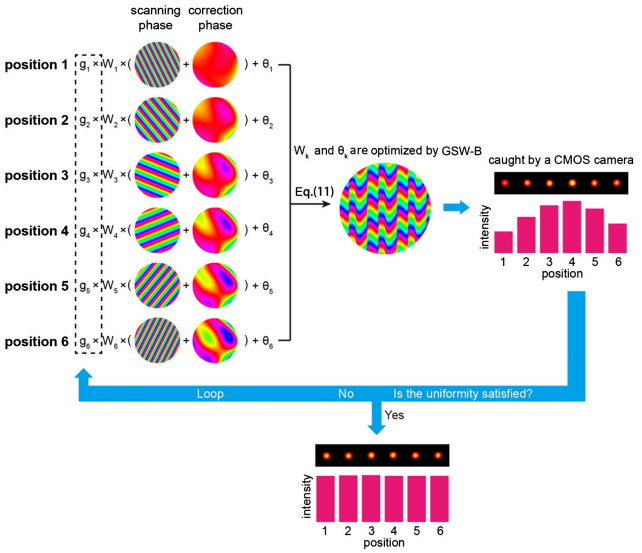

Fig. 2. Schematic for aberration control and intensity homogenization process of the foci array. Scanning phase $\varphi_{\text{scan},k}$ determines the position of the foci; correction phase $\varphi_{\text{AO},k}$ determines the aberration (i.e., "on or off") of the foci; the weight w_k can change the intensity of the foci; θ_k starts with a random phase. g_k is the weight scaling factor calculated by the actual focus intensity captured by the camera. Iteratively correct g_k, w_k, and θ_k to improve the intensity uniformity of the foci.

$$g_k^{(m)} = g_k^{(m-1)} \frac{\bar{I}^{(m-1)}}{I_k^{(m-1)}}, \tag{12}$$

where $I_k^{(m-1)}$ is the intensity of the kth focus captured by the camera, and $\bar{I}^{(m-1)}$ is the average intensity of all foci.

Figure 3(a) shows the generated focal point arrays of 1 to 36 recorded by the camera. It can be seen that all foci arrays actually have 36 foci, but the intensity of the "off" focus drops sharply by introducing aberration. As shown in Fig. 3(b), the intensity

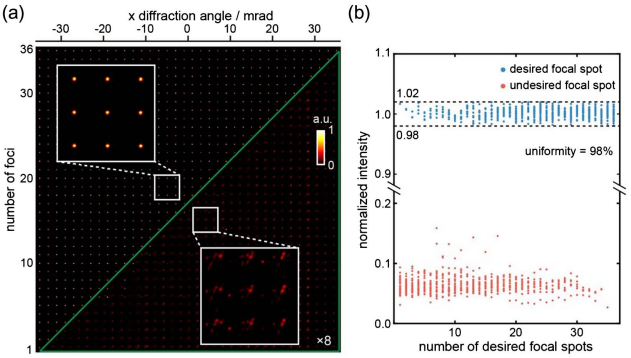

Fig. 3. Results of intensity uniformity for foci arrays with different numbers. (a) shows the foci arrays with a number of foci from 1 to 36, with each row being a focus array. The focus within the green triangle area is the "off" focus, in which the gray value is multiplied by 8. (b) Normalized intensity of all foci. The blue data points represent the "on" foci, and the red data points represent the "off" foci. The intensity uniformity of the "on" foci reaches 98%, and the intensity of the "off" foci is less than 20% of the intensity of the "on" foci.

uniformity of the "on" focus of all foci arrays can reach 98%, and the intensity of the "off" focus is less than 20% of the intensity of the "on" foci. The intensity uniformity of the foci arrays is calculated as

$$U = 1 - \frac{\max(I) - \min(I)}{\max(I) + \min(I)}, \tag{13}$$

where U is the intensity uniformity of the foci and I is the intensity of the foci.

The optical configuration of the scanning system is schematized in Fig. 4. The light source is a fiber femtosecond laser (HR-Femto-IR-50-30, Huaray) with an average power of 30 W at 1035 nm, which is polychromatic. The laser beam is expanded and collimated by a beam-expanding system composed of L1 and L2 ($f_{L1} = 50$ mm, $f_{L2} = 75$ mm). The DMD (DLP650L NIR, Texas Instruments) acts as a blazed grating in this system, with spatial dispersion that needs to be compensated[23]. Therefore, the blazed grating (1158_30 × 13_3_N, Gitterwerk) with a period of 1 μm and a blazed angle of 31° is used to compensate for the spatial dispersion in the center direction of the scanning range. The lenses L3 and L4 ($f_{L3} = 75$ mm, f_{L4}= 200 mm) constitute a 4-f system to match the spatial dispersion produced by the blazed grating and DMD. After the DMD, a Keplerian dispersion compensation module (KDCM), which is a 4-f system with different magnifications at different wavelengths, is configured to compensate for residual dispersion for which the blazed grating cannot compensate[24]. Then, a spatial filter is placed at the Fourier plane of the KDCM to block the unwanted diffraction order. Lastly, the 4-f system composed of lenses L5 and L6 (self-designed, with a magnification of 1×) relays the galvo scanners (MINISCAN-II-10, RAYLASE) to the back-pupil of the objective (CFI Apo NIR 40× W, NA = 0.8, Nikon). To expand the scanning range, the sample is mounted on a motorized precision XYZ stage (ANT130-160-XY-AVL125, Aerotech). The objective, tube lens ($f_{TL} = 180$ mm), and CCD

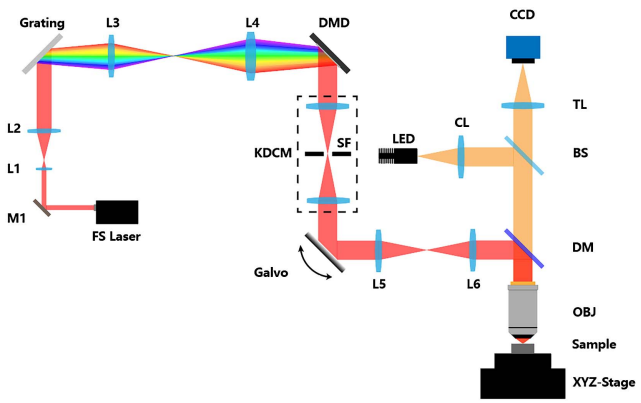

Fig. 4. Optical configuration of the scanning system. FS laser, fiber femtosecond laser; M1, reflectivity mirror; L1-L6, lens; DMD, digital micromirror device; KDCM, Keplerian dispersion compensation module; SF, spatial filter; Galvo, galvanometer scanners; DM, dichroic mirror; OBJ, objective lens; BS, beam splitter; CL, condensing lens; TL, tube lens.

form the microscope system to monitor the cutting process *in situ*. An LED light source (XHP70, XLamp) is coupled into the system through the condensing lens and beam splitter (50:50) to provide illumination for the microscope.

Using our system, we make corneal flaps, which is a step of femtosecond laser-assisted *in situ* keratomileusis (FS-LASIK) *in vitro* porcine eyes. In FS-LASIK as shown in Fig. 5, a circular surface in the cornea with a diameter of about 8 mm needs to be cut by femtosecond laser. It is necessary to make a cylindrical side-cut with the same radius as the circular surface, and its height is about 120 μm. At the same time, the corneal flap pedicle with a width of about 4 mm was reserved for cornea and corneal flap connection. The scanning mode of mosaic splicing is used for circular surface scanning. As shown in Fig. 5(a), the pale blue area is the target scanning surface, each red square (i.e., mosaic) corresponds to an independent scanning field of view, and a circular scanning surface is composed of the mosaics (the mosaic gap is used to distinguish different scanning fields of view, which do not exist in the actual scanning process). There are two types of mosaics, namely mosaic 1 and mosaic 2, as shown in Fig. 5(a). Mosaic 1 is a square scanning surface, which can be scanned with multi-focus parallel raster scanning by the galvo scanners, as shown in Fig. 5(b). Mosaic 2 is located in the area of the edge of the circular surface, which is a typical non-periodic structure that cannot be scanned by the conventional multi-focus parallel raster scanning method. Thus, the scanning strategy described in this paper is adopted in mosaic 2. Figures 5(d)–5(g) show the results of making corneal flaps on the porcine cornea *in vitro* by the multi-focus scanning method described in this paper and the conventional multi-focus scanning method, respectively. The corneal flap made by our system does not yield serrated edges, indicating that our system can achieve multi-focus non-periodic structure scanning. It is also proved that the "on or off" of each focus can be controlled independently by aberration adjustment.

Table 1 compares the time consumption for non-periodic structure scanning (a circular surface with a diameter of 8 mm) by using three scanning methods with the following parameters: the width of mosaic $l_{mosaic} = 320$ μm, the height of mosaic $h_{mosaic} = 400$ μm, the number of mosaics $N_{mosaic} = 416$, scanning points pitch $d = 1.6$ μm, the number of foci $N_{focus} = 8$, the scan frequency of galvo scanners $f_g = 180$ Hz, and the refresh rate of DMD $f_{DMD} = 10.75$ kHz. The mosaic scanning time for the three scanning methods can be calculated as follows:

$$\begin{aligned} T_{single} &= \frac{l_{mosaic}}{2df_g} \cdot N_{mosaic}, \\ T_{multi,DMD} &= \frac{l_{mosaic} h_{mosaic}}{d^2 N_{focus} f_{DMD}} \cdot N_{mosaic}, \\ T_{ourwork} &= \frac{l_{mosaic}}{2dN_{focus} f_g} \cdot N_{mosaic}. \end{aligned} \tag{14}$$

As a scanner, the scanning speed of the DMD is lower than that of the galvo scanner, because the DMD only scans one point

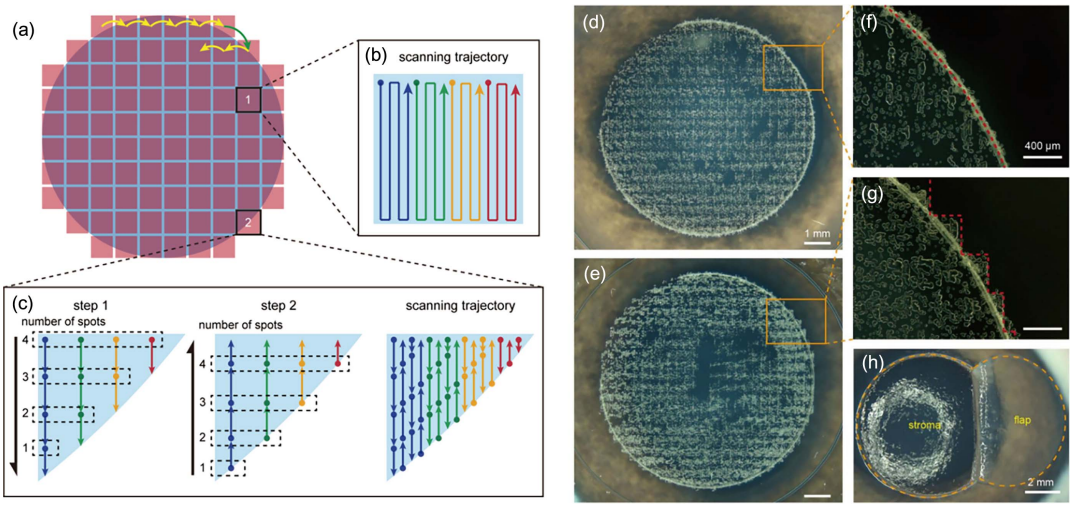

Fig. 5. (a) The scanning mode of mosaic splicing is used to scan a circular surface. The light blue area is the target scanning surface. (b) The mosaic 1, which is completely inside the circle, is a square scanning surface that can be fully scanned with multi-focus parallel raster scanning. (c) The target scanning area of the mosaic 2, which is partly outside the circle, is non-periodic, and thus needs to use the scanning method in Fig. 1. (d) The result of making the corneal flap porcine cornea *in vitro* by the proposed multi-focus scanning method. (e) The result of making the corneal flap by the conventional multi-focus scanning method. (f), (g) The enlarged view of the corresponding part in (d), (e). (h) The result of lifting the corneal flap for (d).

Table 1. Fabrication Time for a Circular Surface with a Diameter of 8 mm under Different Scanning Methods.

Scanning Method	Single-Focus Based on Galvanometers	Multi-Focus Based on DMD	Our Work
Mosaic scanning time	231 s	242 s	29 s
Splicing movement time	15 s	15 s	15 s
Total time	246 s	257 s	44 s

when switching one hologram. The line scanning time of the DMD is given by $T_{\text{line,DMD}} = h_{\text{mosaic}}/(df_{\text{DMD}})$. However, the line scanning time of the galvo scanner is $T_{\text{line,galvo}} = 1/(2f_g)$. Under the scanning parameters used in this work, the scanning time of the multi-focus scanning method based on the DMD is better than the single-focus scanning method based on galvo only when $N_{\text{focus}} > 8$. Our work combines the fast scanning speed of galvo scanners with the flexibility of DMD multi-focus scanning, while achieving non-periodic scanning and improving scanning speed. Compared to the other two methods, the total time-cost of our solution has been reduced by 82% and 83%, respectively.

3. Conclusion

In summary, we present a multi-focus parallel scanning method based on DMDs and galvanometers to realize high-throughput non-periodic trajectory scanning. Meanwhile, the GSW algorithm is improved to realize the independent control of the "on or off" of the foci by introducing and correcting aberration. The method described in this paper can be applied to the field of laser processing and laser medical treatment.

Acknowledgements

This work was supported by the National Key Research and Development Program of China (No. 2022YFC2404500), the National Natural Science Foundation of China (NSFC) (No. 62075077), and the Hubei Province Science and Technology Plan Project (No. 2022BCA049).

References

1. D. Du, X. Liu, G. Korn, *et al.*, "Laser-induced breakdown by impact ionization in SiO_2 with pulse width from 7 ns to 150 fs," Appl. Phys. Lett. **64**, 3071 (1994).
2. S. Kawata, H. Sun, T. Tanaka, *et al.*, "Finer features for functional microdevices," Nature **412**, 697 (2001).
3. W. Denk, J. H. Strickler, and W. W. Webb, "Two-photon laser scanning fluorescence microscopy," Science **248**, 73 (1990).
4. Q. Geng, C. Gu, J. Cheng, *et al.*, "Digital micromirror device-based two-photon microscopy for three-dimensional and random-access imaging," Optica **4**, 674 (2017).
5. C. W. Freudiger, W. Min, B. G. Saar, *et al.*, "Label-free biomedical imaging with high sensitivity by stimulated Raman scattering microscopy," Science **322**, 1857 (2008).
6. K. Wang, Y. Pan, X. Chen, *et al.*, "3-photon fluorescence and third-harmonic generation imaging of myelin sheaths in mouse digital skin *in vivo*: a comparative study," J. Innov. Opt. Health Sci. **15**, 2250003 (2022).
7. K. Wang, S. Tang, S. Wang, *et al.*, "Monitoring microenvironment of Hep G2 cell apoptosis using two-photon fluorescence lifetime imaging microscopy," J. Innov. Opt. Health Sci. **15**, 2250014 (2022).

8. C. W. Freudiger, W. Min, B. G. Saar, *et al.*, "Label-free biomedical imaging with high sensitivity by stimulated Raman scattering microscopy," Science **322**, 1857 (2008).
9. E. N. Glezer, M. Milosavljevic, L. Huang, *et al.*, "Three-dimensional optical storage inside transparent materials," Opt. Lett. **21**, 2023 (1996).
10. K. Bahlmann, P. T. C. So, M. Kirber, *et al.*, "Multifocal multiphoton microscopy (MMM) at a frame rate beyond 600 Hz," Opt. Express **15**, 10991 (2007).
11. D. N. Fittinghoff, P. W. Wiseman, and J. A. Squier, "Widefield multiphoton and temporally decorrelated multifocal multiphoton microscopy," Opt. Express **7**, 273 (2000).
12. F. Wyrowski, "Diffractive optical elements: iterative calculation of quantized, blazed phase structures," J. Opt. Soc. Am. A **7**, 961 (1990).
13. E. D. Diebold, B. W. Buckley, D. R. Gossett, *et al.*, "Digitally synthesized beat frequency multiplexing for sub-millisecond fluorescence microscopy," Nat. Photonics **7**, 806 (2013).
14. H. Li, Y. Cheng, H. Tang, *et al.*, "Imaging chemical kinetics of radical polymerization with an ultrafast coherent Raman microscope," Adv. Sci. **7**, 1903644 (2020).
15. Y. Hayasaki, T. Sugimoto, A. Takita, *et al.*, "Variable holographic femtosecond laser processing by use of a spatial light modulator," Appl. Phys. Lett. **87**, 031101 (2005).
16. L. Yang, A. El-Tamer, U. Hinze, *et al.*, "Parallel direct laser writing of micro-optical and photonic structures using spatial light modulator," Opt. Lasers Eng. **70**, 26 (2015).
17. Q. Geng, D. Wang, P. Chen, *et al.*, "Ultrafast multi-focus 3-D nano-fabrication based on two-photon polymerization," Nat. Commun. **10**, 2179 (2019).
18. B. Jiao, F. Chen, Y. Liu, *et al.*, "Acousto-optic scanning spatial-switching multiphoton lithography," Int. J. Extrem. Manuf. **5**, 035008 (2023).
19. S. Yang, C. Su, S. Gu, *et al.*, "Parallel two-photon lithography achieving uniform sub-200 nm features with thousands of individually controlled foci," Opt. Express **31**, 14174 (2023).
20. R. Di Leonardo, F. Ianni, and G. Ruocco, "Computer generation of optimal holograms for optical trap arrays," Opt. Express **15**, 1913 (2007).
21. W. Lee, "Binary synthetic holograms," Appl. Opt. **13**, 1677 (1974).
22. Y. Wang, H. Li, Q. Hu, *et al.*, "Aberration-corrected three-dimensional non-inertial scanning for femtosecond lasers," Opt. Express **28**, 29904 (2020).
23. J. P. Rice, J. E. Neira, M. Kehoe, *et al.*, "DMD diffraction measurements to support design of projectors for test and evaluation of multispectral and hyperspectral imaging sensors," Proc. SPIE **7210**, 72100D (2009).
24. Q. Hu, Z. Zhou, X. Lv, *et al.*, "Compensation of spatial dispersion of an acousto-optic deflector with a special Keplerian telescope," Opt. Lett. **41**, 207 (2016).